Journal of Electroceramics, 14, 95–102, 2005

Copper Compatible Barium Titanate Thin Films for Embedded Passives

JON IHLEFELD,[1,*] BRIAN LAUGHLIN,[1] ALISA HUNT-LOWERY,[1] WILLIAM BORLAND,[2] ANGUS KINGON,[1] & JON-PAUL MARIA[1]

[1] *Department of Materials Science and Engineering, North Carolina State University, Raleigh, NC 27695*
[2] *DuPont Electronic Technologies, Research Triangle Park, NC 27709*

Submitted March 24, 2004; Revised June 24, 2004; Accepted June 24, 2004

Abstract. Barium titanate thin films have been prepared by chemical solution deposition on 18 μm thick, industry standard copper foils in the absence of chemical barrier layers. The final embodiment exhibits randomly oriented $BaTiO_3$ grains with diameters between 0.1 and 0.3 μm, and an equiaxed morphology. The average film thickness is 0.6 μm and the microstructure is free from secondary or interfacial phases. The $BaTiO_3$ films are sintered in a high temperature reductive atmosphere such that copper oxidation is avoided. Subsequent lower-temperature, higher oxygen pressure anneals are used to minimize oxygen point defects. Permittivities of 2500 are observed at zero bias and room temperature, with permittivities greater than 3000 at the coercive field. Loss tangents under 1.5% are demonstrated at high fields. The $BaTiO_3$ phase exhibits pronounced ferroelectric switching and coercive field values near 10 kV/cm. Temperature dependent measurements indicate a ferroelectric transition near 100°C with very diffuse character. Combining the approaches of the multilayer capacitor industry with traditional solution processed thin films has allowed pure barium titanate to be integrated with copper. The high sintering temperature—as compared to typical film processing—provides for large grained films and properties consistent with well-prepared ceramics. Integrating $BaTiO_3$ films on copper foil represents an important step towards high capacitance density embedded passive components and elimination of economic constraints imparted by traditional noble metallization.

Keywords: barium titanate, copper, ferroelectric, film, capacitor

Introduction

Embedded decoupling capacitors within the layers of a printed wiring board (PWB) offer the ability to free surface space, increase device reliability, and reduce electromagnetic interference and inductance losses. Surface space is freed as capacitors and interconnects are moved to within the PWB, offering additional board area for integrated circuits (IC's) and other active devices. Device reliability increases due to fewer soldered connections between chips, capacitors, and interconnects, and the ability to locate devices directly above decoupling capacitors shortens interconnect lengths. This in turn decreases the lead inductance and increases the maximum frequency of operation [1, 2].

Various groups have deposited chemical solutions of barium titanate on platinized silicon substrates in an effort to develop technologies for dynamic random access memory (DRAM) [3–6]. Though low loss, high capacitance density material can be prepared on Pt surfaces, this technology is not appropriate for embedded passives given the high cost of Pt, the inherent rigidity of typical silicon substrates, and the large series resistance associated with thin Pt electrodes. As an alternative approach, several groups have pursued preparation of high permittivity perovskite dielectrics on thin metal foils [7–9]. The refractoriness and flexibility of the foils provides a substrate amenable to lamination-based embedding, while maintaining compatibility with oxide thin film processing. In most of this research however, leaded dielectrics have been used, primarily due to their ability to be processed at temperatures below 600°C. Though successful and currently pursued for commercialization, leaded dielectrics represent a medium-term solution when considering the ultimate industrial need to eliminate Pb-containing technology. Barium titanate

*E-mail: jfihlefe@unity.ncsu.edu

is an obvious materials choice for lead-free application, but a routine difficulty is presented by its refractoriness and high required crystallization and densification temperatures. Crystallization of barium titanate from metalorganic precursor solutions requires temperatures in excess of 600°C [5] and therefore presents difficulties in preserving the integrity of base metal electrodes during typical perovskite thin film crystallization anneals. It has been shown by Dawley et al. that highly oriented barium strontium titanate (BST) thin films prepared through a chemical solution route can be crystallized on biaxially-oriented nickel tape substrates under a reducing atmosphere [10]. The success of this demonstration resulted from its marriage of thin film and bulk electroceramic technologies [11–13]. In this report, we build upon this base metal electrode approach and demonstrate the deposition of pure barium titanate via the chemical solution deposition (CSD) technique on bare copper foils. In doing so, we provide a direct means through which high capacitance density dielectrics can be integrated into printed wiring board technology using a complement of materials and processes economically compatible with the extremely cost competitive PWB industry.

Experimental Procedure

A precursor solution was prepared by combining Ba acetate dissolved in glacial acetic acid and titanium isopropoxide reacted with acetylacetone as a chelating agent in an equimolar ratio. The bulk solution was diluted to 0.3 molar with methanol and diethanolamine (DEA). The incorporation of diethanolamine provides a strain relief mechanism during removal, thereby facilitating improved morphology [14].

The precursor solution was spin coated onto 18 μm thick bare copper foils at 3000 rpm for 30 seconds followed by a hot-plate drying step at 250°C for 7 minutes. This process was repeated until the desired thickness was achieved—in this case, three to four layers were applied. The films were crystallized by annealing at 900°C for 30 minutes in an atmosphere consisting of a mixture of reagent grade nitrogen and hydrogen containing forming gas bubbled through 25°C water. These conditions are sufficient to provide an environment with an oxygen partial pressure (pO_2) of 10^{-9} atmospheres and a total pressure of 1 atmosphere.[1] The resulting film thickness after firing was 0.6 μm. A reoxidation anneal was performed at 600°C under vacuum with a controlled oxygen leak at a total pressure of $\sim 10^{-7}$ atm O_2 for 30 minutes. Platinum top electrodes $\sim 10^{-4}$ cm^2 and 100 nm thick, were deposited by DC magnetron sputtering through a shadow mask.

Film crystallinity and phase development were studied with a Bruker AXS D-5000 X-ray diffractometer equipped with a GADDS area detector. Film surface composition was studied with X-ray photoelectron spectroscopy (XPS) in a vacuum chamber at 10^{-10} torr equipped with a VG Clam semi-hemispherical electron spectrometer and a dual anode X-ray source. The source used in the XPS scan was Al Kα. The survey and copper spectra were obtained with 50 and 20 eV pass energy, respectively. A CP-Research Thermomicroscopes Autoprobe scanning probe microscope and a Hitachi S3200 scanning electron microscope were used to study the $BaTiO_3$ surface morphology. A JEOL 2010F transmission electron microscope (TEM) was used to image the cross-sectional structure of the films. A wedge polishing technique was used to prepare all TEM samples. Dielectric properties, including dielectric constant and loss tangent were measured with a Hewlett-Packard 4192A Impedance Analyzer and an MMR Technologies Inc. cryogenic temperature stage. Dielectric constant versus voltage curves were developed with DC biases ranging from -10 to 10 V with an oscillator amplitude of 0.05 V and a 100 kHz frequency. Dielectric constant versus temperature was measured in the range of 100 to 500 K at zero DC bias and similar oscillator conditions. Leakage current density was measured using a Keithley 617 Programmable Electrometer at room temperature. Current densities were measured in the range of -10 to 10 V with a time delay at voltage of 15 seconds between each reading to minimize the contribution of ferroelectric switching to the overall measured current. Device reliability was measured by poling the devices at 3 V for 10 seconds and then measuring the capacitance density after allowing the capacitor to hold for 10 seconds at zero bias.

Results and Discussion

Figure 1 shows an X-ray diffraction pattern for a typical $BaTiO_3$ sample prepared on copper foil. The pattern exhibits narrow peak widths, random orientation, and a low, flat background noise level. These features are more consistent with well-prepared ceramic material than with traditionally processed thin films. Figure 1 also illustrates that no Cu_2O or CuO phases are detected

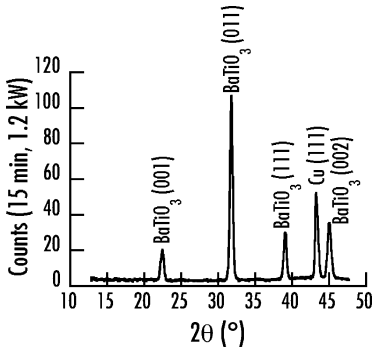

Fig. 1. θ-2θ X-ray diffraction pattern of a 3 layer ($\sim$0.6 μm) $BaTiO_3$ film on 18 μm thick Cu-foil.

following the crystallization process. This result is predicted by thermodynamic calculations of the Cu–O_2–Cu_2O system at 900°C and a $pO_2 < 10^{-9}$ atm [15]. Note that the area detector used provides a particularly high sensitivity for the detection of poorly crystalline or low volume fraction second phases, thus the absence of scattering events not attributable to Cu or $BaTiO_3$ is a strong indication of an abrupt Cu/$BaTiO_3$ interface over a large sampling area.

The mobility of copper atoms at 900°C could allow copper to diffuse through the $BaTiO_3$ film and present pathways for shorts to develop between the top and bottom electrodes. Figure 2 shows the XPS data obtained to investigate diffusion of copper through the $BaTiO_3$ film. The data shows that copper is present on the surface of the film in trace concentrations. However

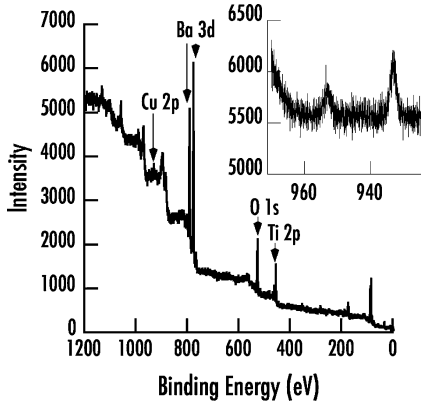

Fig. 2. XPS spectrum from $BaTiO_3$ deposited on copper foils after crystallization and annealing steps. Inset shows close up of XPS spectrum for copper 2p peaks.

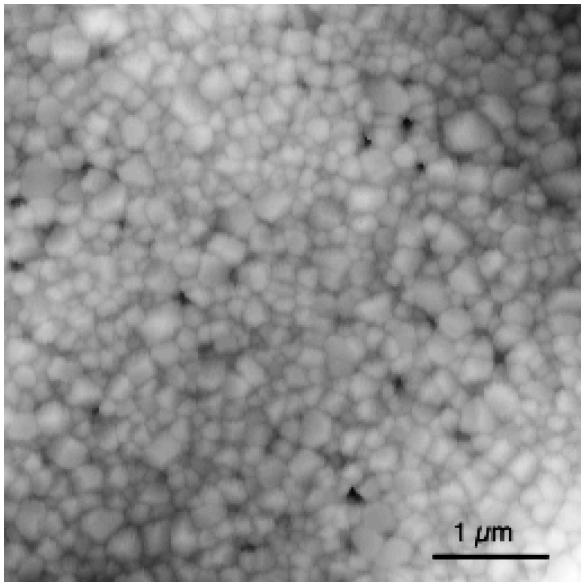

Fig. 3. Tapping mode AFM surface image of a $BaTiO_3$ thin film deposited on Cu-foil.

it should be noted that the equilibrium vapor pressure of copper at 900°C is $\sim 10^{-8}$ atmospheres. This relatively high vapor pressure is likely to condense on the film surface during cooling.

Figure 3 is a topographic image of a $BaTiO_3$ film surface collected using atomic force microscopy in a 5 μm by 5 μm scan size. The surface microstructure present reflects equiaxed grains ranging in diameter from 0.1 μm to 0.3 μm, with an average of 0.2 μm.

A bright field TEM image is shown in Fig. 4. This micrograph verifies that the equiaxed grain morphology is present through the thickness of the film. It is interesting to note that there appears to be a grain boundary that nearly divides the $BaTiO_3$ layer. This suggests that crystallization occurs at two film interfaces, growth proceeds until the individual fronts meet near the film center, and the impact of the number of spun-on organic layers is small. This results in a film that is on average two grains thick. Here we note that this observation is in contrast to previous reports where homogeneous nucleation was the preferred crystallization pathway for $BaTiO_3$ thin films [5, 16]. We speculate that this difference results in part from the highly reducing atmosphere used to extract organic and crystallize the BT layers. High resolution TEM reveals no interfacial phases present at the $BaTiO_3$-copper interface, as is supported by the lack of additional phases present in the X-ray diffraction data.

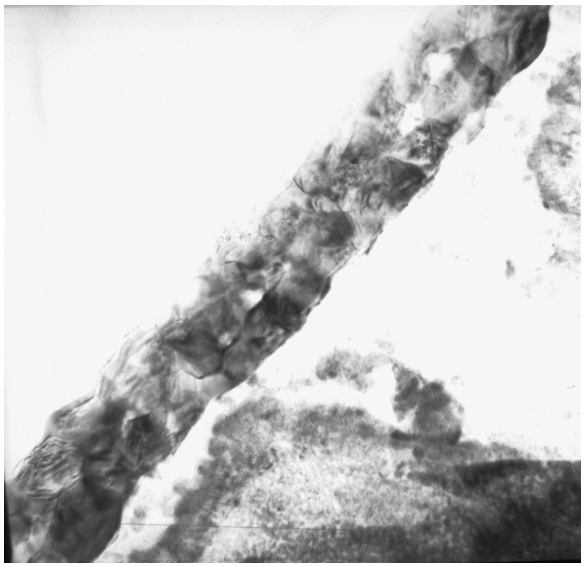

Fig. 4. Bright field TEM micrograph of a cross-sectioned $BaTiO_3$ thin film deposited on Cu-foil.

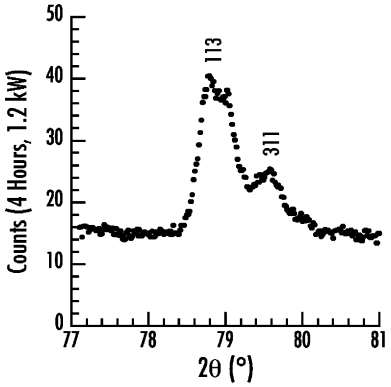

Fig. 5. High-resolution θ-2θ X-ray diffraction pattern of the (113) and (311) reflections of a $BaTiO_3$ thin film deposited on Cu-foil.

Given the modest grain sizes observed, it is expected that the perovskite $BaTiO_3$ will be ferroelectric and of tetragonal symmetry. A high-resolution X-ray diffraction pattern was collected for the (113) and (311) peaks and clearly demonstrates splitting. Figure 5 illustrates this data and verifies the non-cubic symmetry.

As physical characterization reveals a microstructure and crystal structure comparable to fine-grain ceramics, similar electrical properties are expected, i.e., dielectric constant (K) values in excess of 10^3 and clear evidence of hysteresis. This is in contrast to most examples of $BaTiO_3$ films prepared on Pt-Si substrates. Figure 6 shows the temperature dependence of K for a 600 nm thick film (the sample from which the TEM image in Fig. 4 was taken). As this film thickness is well known, accurate values of permittivity could be determined. This data is co-plotted with ceramic and thin film data sets such that the properties can be appreciated in the proper context. For bulk ceramic reference, we use the well-known Arlt and Frey results comparing, in so far as possible, permittivity vs. temperature traces for similarly sized grains [17, 18]. Alternatively, for thin film reference, we use data sets from Hoffman and Parker [5, 19]. In all cases, a representative crystal size is listed. With this plot we clearly appreciate a favorable comparison between the current $BaTiO_3$ films and ceramics. The ultra-large permittivities of Frey have not been duplicated, however, the highly reducing atmospheres used to preserve the copper substrates leave a dielectric with higher point defect concentrations which tend to eliminate some of the extrinsic dielectric contributions and reduce overall permittivity. Note also that the permittivities achieved are significantly higher than observed for the thin film examples. Figure 7 shows the field dependence for samples processed under these conditions, room temperature permittivity values of 2500 are achieved at zero bias with values approaching 3200 at the coercive field of 10 kV/cm, with a 10× electrical tunability.

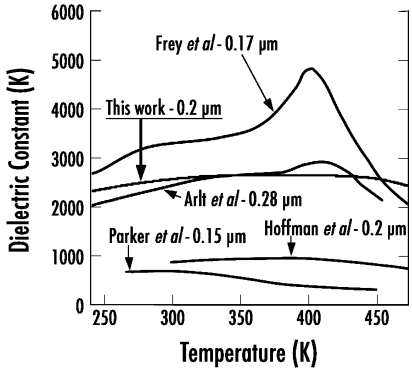

Fig. 6. Comparison of the temperature dependence of permittivity between a $BaTiO_3$ thin film on Cu-foil and $BaTiO_3$ ceramics and thin films from several literature sources [5, 18–20].

These samples, however, did not exhibit high capacitor yield, mostly attributable to the existence of porosity. By tailoring the solution chemistry and deposition procedure to optimize the organic removal process, greatly improved yield and electrical property

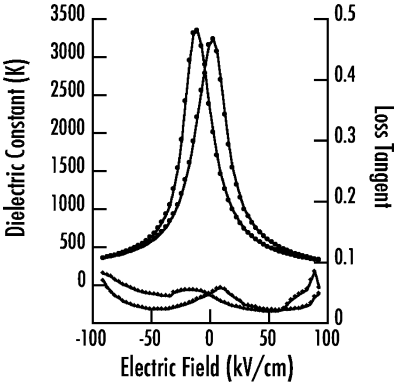

Fig. 7. Field dependence of permittivity and loss tangent of a 3-layer (600 nm) $BaTiO_3$ film on Cu-foil.

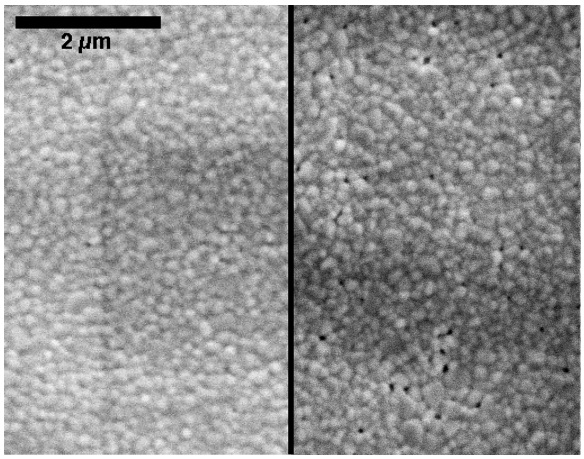

Fig. 8. Secondary and backscatter electron SEM micrographs comparing the film morphology of DEA modified $BaTiO_3$ thin films on Cu-foil on the left and non-DEA containing $BaTiO_3$ on Cu-foil on the right.

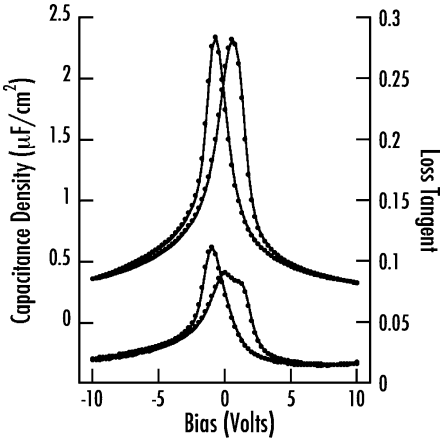

Fig. 9. Voltage dependence of capacitance density and loss tangent of $BaTiO_3$ thin film on Cu-foil with optimized microstructure.

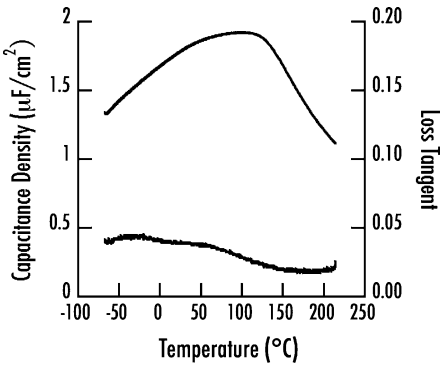

Fig. 10. Temperature dependence of the capacitance density and loss tangent of a $BaTiO_3$ thin film on Cu-foil with optimized microstructure.

consistency was achieved. An improved microstructure, including a decrease in film porosity, is attributed to these results as shown in the SEM micrograph in Fig. 8. The left side of the figure shows the microstructure of a DEA modified $BaTiO_3$ film, compared to a film deposited without the addition of DEA. A distinct decrease in the film porosity is noted in the DEA modified films. Field dependent capacitance density data is shown for such samples in Fig. 9. Note the low loss tangent values and saturated capacitance density traces are maintained to high electric fields. The temperature response of capacitance density and loss tangent for the optimized film is shown in Fig. 10. In Figs. 9 and 10 capacitance density values are given as the absolute film thickness is not accurately known. In Fig. 10 the ferroelectric transition is observed close to the bulk value of 130°C, while a slope change in near 5°C hints of the orthorhombic-tetragonal phase transition.

The leakage current density versus applied bias of these films is shown in Fig. 11. While the leakage current density is generally greater than desired in many capacitor applications, it should be reiterated that these are pure barium titanate films processed under reducing conditions. As such, the reoxidation is unlikely to be complete and the presence of easily ionized oxygen vacancies will contribute to the dc leakage. As is the case in bulk $BaTiO_3$ capacitors, it will probably be necessary to engineer the overall defect chemistry by

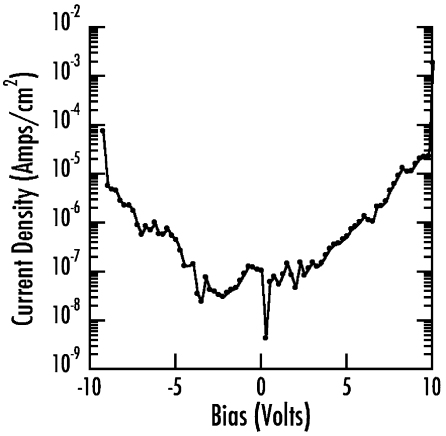

Fig. 11. Voltage dependence of leakage current density of a $BaTiO_3$ thin film on Cu-foil with optimized microstructure.

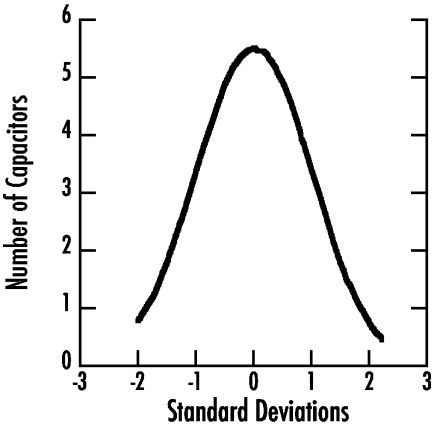

Fig. 12. Plot demonstrating the normal distribution and small variance of capacitance for 39 randomly selected capacitors.

aleovalent doping to achieve the desired insulation resistance. This will be the focus of future work and has not been addressed at this time.

Given the low loss tangents at high field and high dielectric constant of the $BaTiO_3$ films on copper foils, it is unlikely that the copper identified on the surface of the films by XPS is in a continuous path from the bottom electrode to the top. If direct paths were formed, it would be expected that short circuits would develop between top and bottom electrodes. Copper oxide would be expected to act as a 2^+ B site dopant and function as an acceptor ion in the $BaTiO_3$ host lattice [20, 21]. Such acceptor doping would be expected to harden the electromechanical response by lowering the permittivity and increasing the coercive field - neither consequence is apparent [22]. Specifically, we would expect large coercive field values. In the present case, however, 10 kV/cm is observed. This value is comparable to those reported for pure barium titanate ceramics [23]. The dependence of T_c is not useful for elucidating the presence of Cu doping as its value changes very little up to the solubility limit [24, 25]. Collectively, these arguments do not eliminate the possibility of Cu diffusion, however, they do suggest that if copper is present, its concentrations are small and its impact is not problematic. Ultimately, identifying the specific concentration of copper in the BT films and its influence will be necessary to fully understand device performance.

Figure 12 illustrates the normalized distribution of capacitance density for 40 randomly selected capacitors from a representative section of $BaTiO_3$ coated foil. Of 40 selected capacitors, there was one short circuit. Spot values of capacitance were taken for each of the 39 devices at zero volts after a 10 second exposure to 3 V to minimize the effect of hysteresis. The distribution of capacitance density for these capacitors was normal with a mean of 1.94 μF/cm^2 and a standard deviation of 0.07 μF/cm^2. All capacitance densities fell within two standard deviations of the mean, indicating a reproducible product with a tight distribution. From this we see that the concept of $BaTiO_3$ on comparatively rough copper foils represents a viable approach for a manufacturable embedded capacitor.

The barium titanate films grown on copper substrates exhibit much higher permittivities than do barium titanate films prepared by many other groups. This condition is true for materials with grain sizes similar to, or smaller than the sizes presented in this study. Additionally, the room temperature permittivities of most published barium strontium titanate films are again lower than the values presented here [26–33]. (Note that BST films with Sr compositions above $\sim$30% should have room temperature values greater than expected for pure barium titanate.) These observations provide the authors with the ability to comment on scaling effects in ferroelectric films. In numerous literature cases, authors explain low permittivities and reduced domain contributions through a size effect, or physical scaling mechanism. Though many thin film reports have demonstrated a correlation between physical dimension and permittivity, the permittivities of well-prepared ceramics have not been appreciated in thin layers. Most often, a plateau in properties is reached,

beyond which additional increases in thickness provide minimal gain in K. We hypothesize that film thickness is only one contribution to the size effects phenomenon, while the other perhaps more important contribution is processing temperature.

One commonality shared by most ceramic processes but limited in most thin film processes is exposure to high temperatures. This exposure can occur in either the calcinations of powder, or the densification of a ceramic, but temperatures in excess of 900°C are nearly always performed. In contrast, thin film processing conditions seldom achieve these temperatures, especially when metallic bottom electrodes are used. When chemical compatibility is not a concern, thin film processing temperatures are routinely limited by substrate presence. The differences in thermal expansion coefficients of ferroelectric films, noble metal electrodes, and common semiconductor substrates (especially Si), impart residual strains that promote film delamination, thermophysical instabilities (like Pt hillocking), or cracking when certain threshold temperatures are achieved. Consequently, for example, with Si substrates thin film processing temperatures are limited. In the presence of these temperature limitations, thin films do not receive the same kinetic opportunity afforded to powder processed ceramics, and similarly refined crystalline structures are unlikely.

In this report, the use of copper substrates provides for process temperatures much higher than typically available to thin films. Consequently, we propose that a barium titanate crystal structure and microstructure more consistent with a high temperature processed ceramic is achieved, and that similarly consistent electrical properties are observed. Most notably, we show room temperature permittivities above 2500, coercive fields below 10 kV/cm, pronounced domain wall contributions, sharp switching, electrical tuning of 10×, and low loss tangents at high field. We attribute the magnitudes of these values and their similarity to the properties of bulk ceramics to the 900°C processing temperature. Clearly additional work is needed to understand scaling effects, but this report improves the link between the structure, process, and properties of barium titanate thin films and bulk ceramics.

Conclusions

This work demonstrates the deposition of a chemical solution of barium titanate on copper foils for use as an embedded component in a PWB. By controlling the partial pressure of oxygen in each step of high temperature processing, a barium titanate film with bulk ceramic microstructure can be formed on copper foils with no interfacial layer. Atomic Force Microscopy revealed a surface microstructure with grain sizes ranging from 0.1 μm to 0.3 μm in diameter. X-ray diffraction showed a split (113) reflection consistent with the tetragonal perovskite structure. Shadow mask defined capacitors exhibit dielectric constants of 2500 at zero bias and room temperature and loss tangent values less than 1.5% at high fields. These characteristics represent a 1000× improvement over currently available low-mass, large-area, embeddable capacitor technologies.

Acknowledgments

The authors would like to acknowledge the support of DuPont Electronic Technologies, Research Triangle Park, North Carolina and the work of Dr. Ramon Collazo at North Carolina State for his XPS measurement and analysis.

Note

1. The H_2 and O_2 impurities in reagent grade nitrogen ($\sim 10^2$ ppm) establish an equilibrium with the H_2O vapor and yield an effective pO_2 of $\sim 10^{-8}$ atm @ 900°C.

References

1. A. Madou and L. Martens, *IEEE Transactions on Electromagnetic Compatability*, **43**(4), 549 (2001).
2. L.-S. Chen, S.-L. Fu, and K.-D. Huang, *Jpn. J. Appl. Phys.*, **37**(2) No. 10B, L1241 (1998).
3. B. Lee and J. Zhang, *Thin Solid Films*, **338**, 107 (2001).
4. H.-Y. Tian, W.-G. Luo, X.-H. Pu, and A.-L. Ding, *J. Matl. Sci. Letters*, **19**, 1211 (2000).
5. S. Hoffmann and R. Waser, *J. Eur. Cer. Soc.*, **19**, 1339 (1999).
6. N.V. Giridharan, R. Varatharajan, R. Jayavel, and P. Ramasamy, *Mat. Chem. Phys.*, **65**, 261 (2000).
7. J.-P. Maria, K. Cheek, S. Streiffer, S.-H. Kim, and A. Kingon, *J. Amer. Cer. Soc.*, **84**(10), 2436 (2001).
8. K. Saegusa, *Jpn. J. Appl. Phys.*, **36**(11) Part 1, 6888 (1997).
9. Q. Zou, H.E. Ruda, and B.G. Yacobi, *Appl. Phys. Lett.*, **78**(9), 1282 (2001).
10. J.T. Dawley and P.G. Clem, *Appl. Phys. Lett.*, **81**(16), 3028 (2002).
11. J.M. Herbert, *Trans. Br. Cer. Soc.*, **62**(8), 645 (1963).
12. J.M. Herbert, *Proc. IEE*, **112**(7), 1474 (1965).

13. I. Burn and G.H. Maher, *J. Mater. Sci. Eng*., **10**, 633 (1975).
14. J.T. Dawley, P.G. Clem, M.P. Siegal, D.R. Tallant, and D.L. Overmyer, *J. Mater. Res.*, **17**(8), 1900 (2002).
15. D.R. Gaskell, *Introduction to the Thermodynamics of Materials* (Taylor & Francis Books, Inc., New York, 2003), p. 359.
16. R.W. Schwartz, P.G. Clem, J.A. Voigt, E.R. Byhoff, M. Van Stry, T.J. Headley, and N.A. Missert, *J. Am. Ceram. Soc*., **82**(9), 2359 (1999).
17. G. Arlt, D. Hennings, and G. de With, *J. Appl. Phys.*, **58**(4), 1619 (1985).
18. M.H. Frey, Z. Xu, P. Han, and D.A. Payne, *Ferroelectrics*, **206–207**, 937 (1998).
19. C.B. Parker, J.-P. Maria, and A.I. Kingon, *Appl. Phys. Lett.*, **81**(2), 340 (2002).
20. M. Rekas, *Solid State Ionics*, **20**, 55 (1986).
21. H.T. Langhammer, T. Müller, R. Böttcher, and H.-P. Abicht, *Solid State Sciences*, **5**, 965 (2003).
22. B. Jaffe, W.R. Cook Jr., and H. Jaffe, *Piezoelectric Ceramics* (Academic Press Limited, Marietta, OH, 1971), p. 159.
23. H.B. Sharma and A. Mansingh, *J. Mat. Sci*., **33**, 4455 (1998).
24. T. Sakudo, *J. Phys. Soc. Japan*, **12**, 1050 (1957).
25. A. Inoue, M. Iha, I. Matsuda, H. Uwe, and T. Sakudo, *Jpn. J. Appl. Phys*., **30**(9B), 2388 (1991).
26. T. Hayashi, N. Ohji, K. Hirohara, T. Fukunaga, and H. Maiwa, *Jpn. J. Appl. Phys*., **32**(1, 9B), 4092 (1993).
27. C. Basceri, S.K. Streiffer, A.I. Kingon, and R. Waser, *J. Appl. Phys*., **82**(5), 2497 (1997).
28. C.-R. Cho, S.-I. Kwun, T.-W. Noh, and M.-S. Jang, *Jpn. J. Appl. Phys*., **36**(1, 4A), 2196 (1997).
29. H.B. Sharma and A. Mansingh, *J. Mat. Sci*., **33**, 4455 (1998).
30. S.K. Streiffer, C. Basceri, C.B. Parker, S.E. Lash, and A.I. Kingon, *J. Appl. Phys*., **86**(8), 4565 (1999).
31. J.-G. Cheng, X.-J. Meng, B. Li, S.-L. Guo, J.-H. Chu, M. Wang, H. Wang, and Z. Wang, *Appl. Phys. Lett.*, **75**(14), 2132 (1999).
32. J. Thongrueng, K. Nishio, Y. Watanabe, K. Nagata, and T. Tsuchiya, *Pub. Cer. Soc. Jpn*., **181–182**, 85 (2000).
33. R. Thomas, V.K. Varadan, S. Komarneni, and D.C. Dube, *J. Appl. Phys*., **90**(3), 1480 (2001).